International Conference on Advances in Structural and Geotechnical Engineering

ICASGE'17

27-30 March 2017, Hurghada, Egypt

Structural Performance of Self-compacted Concrete Beams with Rectangular Perforations

Hamida Ibrahim[1], Hamdy M.Afefy[2], Nesreen M. Kassem[3], Salah El-Din F. Taher[4]

[1] *Graduate student, Faculty of Engineering, Tanta University, Egypt*
E-mail: hamidaibrahim2007@yahoo.com
[2] *Associate Professor, Faculty of Engineering, Tanta University, Egypt*
E-mail: hamdy.afefy@f-eng.tanta.edu.eg
[3] *Associate Professor, Faculty of Engineering, Tanta University, Egypt*
E-mail: nesreen.kassem@f-eng.tanta.edu.eg
[4] *Professor, Faculty of Engineering, Tanta University, Egypt*
E-mail: salah.taher@f-eng.tanta.edu.eg

ABSTRACT

This paper verifies experimentally the structural performance of self-compacted perforated beams having rectangular perforations. Three perforations sizes have been considered; namely, 200 x 200, 200 x300 and 200 mm x400 mm, respectively. The perforation depth to the beam total depth was kept constant for the three sizes (0.50). These perforations correspond to mass loss percentages of about 24, 29 and 31%, respectively, compared to that of the solid beam. Thus, one solid control beam along with three perforated beams having the three perforation sizes were prepared and tested up to complete failure. The perforation sizes of 200x200 and 200x300 enabled the perforated beams to manifest higher ultimate capacities by about 11% and 1.2% compared to that of the solid beam. On contrary, the perforated beam of perforations dimensions 200 x 400 showed lower ultimate capacity by about 17% compared to that of the solid beam. In addition, the sharp edges of the rectangular perforations enforced the perforated beams to be failed due to shear at the first web-post for all perforated beam.

Keywords: RC beams, Self-compacted concrete, Experimental study, perforated beam, Ductility.

INTRODUCTION

The construction of modern buildings requires providing web opening in the web of the beams in order to accommodate pipes for essential facilities such as air conditioning, electricity, telephone, and computer network [1]. The web opening could take any shape, however, the most favorable shapes are the rectangular and the circular openings [2]. Although, the ducts of air-conditioning have usually rectangular shapes, and they are accommodated in rectangular openings through the beams [3].

With respect to the opening's size, many researchers specified the opening as small and large one without giving a clear range for definition of size. Mansur and Hasant [4] considered the circular and square opening as small openings. While Somes and Corley [5] specified the circular opening as large one when the ratio of opening diameter to the total depth of beam exceeds 0.25. On the other hand some researchers considered that the fundamental classification of opening as either small or large one depends on the structural behavior of the beam [5, 6]. If the opening is small enough to keep the same behavior of beam, or if the usual beam theory applies, the opening will be classified as small opening. If there is a change in the behavior of the beam due to the presence of openings, then the openings may be classified as a large openings.

Self-compacted concrete (SCC) is a special form of concrete which is used for general applications. The main advantage that SCC has over traditional concrete is its high followability, workability, and passing ability [7-10]. Experimental investigations have been carried out on beams with different rectangular and square openings in order to predict the effect of providing such openings on the overall behavior of such beams. For the current research work, openings with height of 0.5 of the beam depth have been studied, which have

different widths of 200, 300 and 400 mm that corresponding to mass reduction of about 24.24%, 28.57% and 30.73%, respectively.

EXPERIMENTAL WORK PROGRAM

Test beams

The experimental work program consisted of four simply supported beams. The first beam is a solid beam representing a reference (control) beam, while the second beam contained eight square openings of 200 mm side length. The third beam contained six rectangular openings of dimensions 200x300 mm, and the fourth one contained five rectangular openings of dimensions 200x400 mm. Thus, all perforated specimens had the same opening depth of 200 mm. Table 1 shows nomenclature and characteristics of all beams.

Table 1: Test matrix

Specimens	Perforation size, mm	Volume reduction %	Objectives
B1	N/A	0	Control solid beam
B2	200 x 200	24.24	Perforated beams with different perforations sizes
B3	200 x 300	28.57	
B4	200 x 400	30.73	

All beams had the same concrete dimensions where the total length of the beams was 3,500 mm while the center to center span was 3,300 mm. The beams cross-section was 150 mm width by 400 mm total depth. The main steel reinforcement of the beams was two high tensile steel bars of 16 mm diameter, while the secondary steel was two high tensile steel bars of 10 mm diameter. The stirrups were mild steel bars of 8 mm diameter and spaced every 100 mm as shown in Fig. 1. For all perforated beams, two high tensile steel bars of 10 mm diameter were provided below and over the perforations as depicted in Fig. 1.

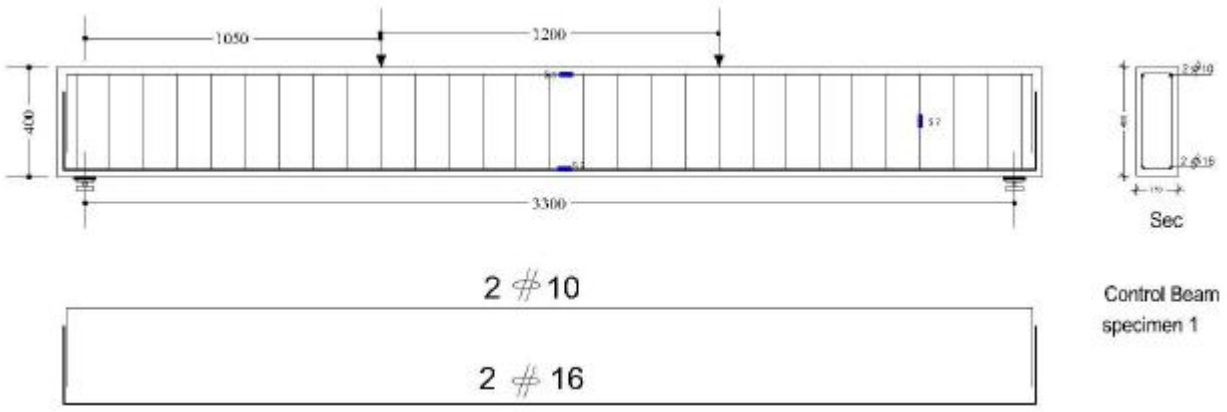

(a) Beam B1 (control)

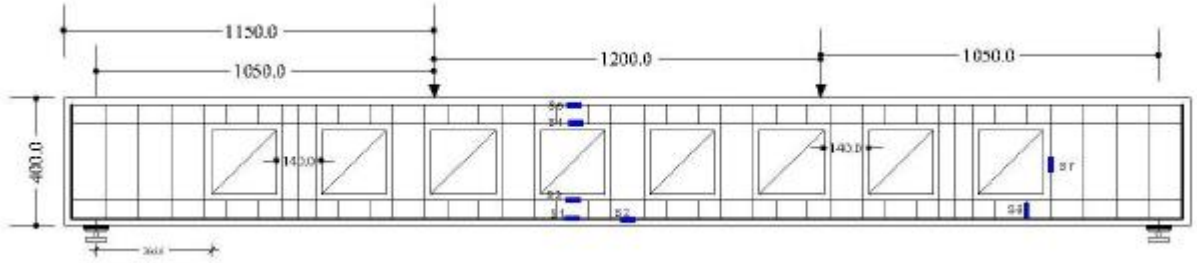

(b) Beam B2 of perforations dimensions 200x200

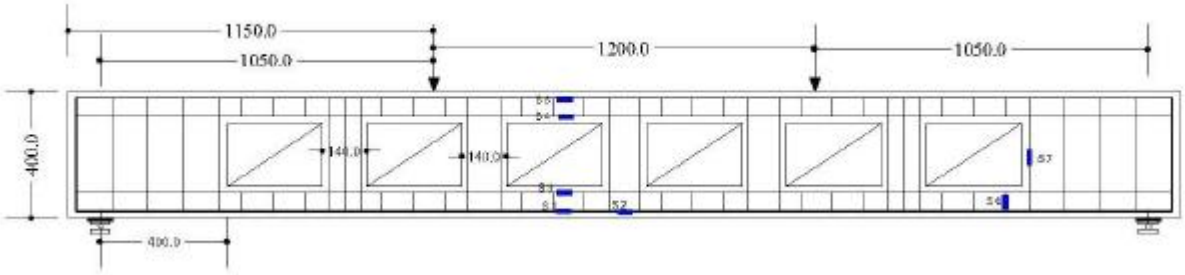

(c) Beam B3 of perforations dimensions 200x300

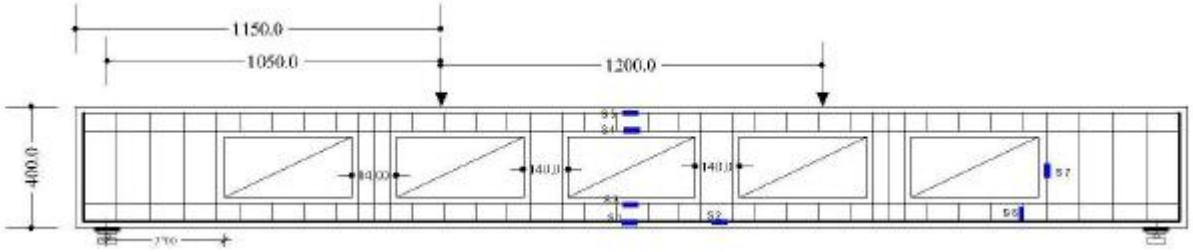

(d) Beam B4 of perforations dimensions 200x400

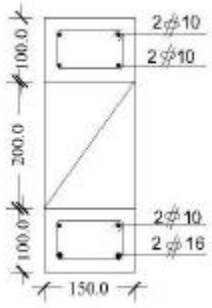

(e) Reinforcement detailing at opening location

Fig. 1: Concrete dimensions and reinforcement detailing for the tested beams.

Material properties

Concrete

The used concrete was self-compacted concrete (SCC) with target cube strength of 45 MPa. It made from ordinary Portland cement (Type I), local natural sand, coarse aggregate of maximum size of 10 mm, ordinary clean tap water, superplasticizer based on poly-carboxylic ether and silica fume with a mixture proportions as recommended by Okamura and Ozawa [7] and listed in Table 2. The actual compressive strength and tensile strength of the used concrete were determined at the testing day using the standard cubes and cylinders cast with the concrete beams. The average compressive cube strength was 49.84 MPa, while the indirect tensile strength obtain from splitting cylinder test was about 5.23 MPa.

A concrete mix can only be classified as self-compacted concrete if it has the following properties; filling ability i.e., the ability to flow under its own weight without vibration; passing ability i.e., the ability to flow through heavily congested reinforcement under its own weight, and segregation resistance [8-10].In order to characterize the properties of SCC as previously mentioned, three tests were performed based on EFNARC specification and guidelines [11]. Table 3 shows the test results of SCC.

Table 2: Mix proportions of Self-compacting RC beams material for one cubic meter (kg/m^3)

Concrete mix	W/B*	Cement	Sand	Coarse aggregates	Water	Silica fume	Super- plasticizer
SSC	0.41	400	800	930	180	40	5.6

* W/B is the water/ binder ratio, B = cement + silica fume

Table 3: The test methods for the workability properties and the trial results of SCC.

Method	Property	Unit	Min.	Max.	Trial Result
Slump flow	Filling ability	mm	600	800	710
V- funnel	Filling ability	Sec	6.00	12.00	9.00
L- Box	Passing ability	-	0.80	1.00	0.9
V-funnel at 5 min	Segregation Resistance	Sec	0.00	3.00	2.1

Reinforcing steel

The used longitudinal steel bars were high tensile steel of 10 mm, 16 mm diameters and the transverse steel bars were plain smooth of 8 mm diameter. In order to determine the mechanical properties of the used steel bars, tensile tests were performed on three typical specimens. The mean values of such properties were summarizes in Table 4.

Table 4: Steel properties

Type of steel bars	Mild Steel (Smooth)	High Tensile Steel (Deformed)	
Diameter, mm	8.00	10.00	16.00
Cross-section Area , mm ^{2}	50.27	78.54	201.06
Yield strength f_y , MPa	285.00	410.00	420.00
Ultimate strength f_u, MPa	410.00	578.00	622.00
Young's modulus E , GPa	201.00	202.44	202.72
Strain at yield ε_y ,(x 10 $^{-3}$ mm / mm)	1.42	2.03	2.07

Test setup and instrumentation

One bay of three-dimensional steel frame as presented in Fig. 2 was equipped and then used to carry out the testing. Three 100 mm LVDTs were used in order to measure the vertical deflection at three locations (0.16, 0.33 and 0.5 beam' span) along the beam as illustrated in Fig. 2. While, 6 mm strain gauges were used in order to measure the developed normal strains in the internal reinforcement at different locations shown in Fig. 1. In addition, three 100 mm gauge length Pi-gauge was used in order to measure the developed deformations on the concrete surface as shown in Fig.2. Hence, the concrete strains could be obtained. The beam was loaded at two points of the beam through a loading steel beam in which the loading was repeated. Therefore in several steps the beam was loaded up to failure. The load on the beam was measured by a load cell of 200 KN capacity. After each loading-unloading step, the vertical deflections, the Pi-gauge readings, the developed normal strains in the longitudinal steel bars were recoded and stored using an automatic data logger unit (TDS-150).

Fig. 2: Test setup and instruments.

TEST RESULTS AND DISCUSSIONS

All beams were subjected to non-reversal repeated loading up to complete failure by either flexural or shear mode. The first cycle of loading was ended when the major flexural crack width reached up to 1 mm. Then the acting load was released and the following cycle was performed. Table 5 summarizes the recorded failure characteristics after complete collapse of all beams. In addition, in the following, detailed analysis is conducted considering the crack pattern and modes of failure, load-deflection response, developed tensile normal strain on the internal main steel and the efficiency of the adopted perforations' configurations.

Table 5: Experimental failure characteristics after complete collapse for all beams

Specimen	Perforation size , mm x mm	Ultimate Load, kN	Frist flexural cracking load, kN	Frist shear cracking load, kN	Max. mid-span Deflection mm	Max strain at main steel, micro-strain	Mode of failure
B1	N/A	125.0	35	97	85.1	4843	Flexural failure
B2	200 x 200	138.4	31	59	23.7	1596	Shear failure
B3	200 x 300	126.5	31	49	14.1	2113	Shear failure
B4	200 x 400	104.0	30	37	19.8	2852	Shear failure

Crack pattern and modes of failure

The cracking pattern and the mode of failure for the control solid beam was regular flexural cracking and mode of failure. The beam started to develop flexural cracks at a jacking load of about 35 kN. With proceeding with loading, flexural cracks were spread along the tensile side up to the commencement of shear cracking at a jacking load of about 97 kN. The loading was continued till the width of the major crack approached 1 mm then the load was released up to zero load, and then the second cycle was performed and stopped when the beam could not sustain more loading. Thus the third cycle was applied up to complete failure of the beam owing to flexural mode of failure as depicted in Fig. 4(a).

As for the perforated beams, the flexural cracks started to show up at lower load level compared to that of the solid control beam (B1). The first flexural cracking loads are 31, 31, and 30 kN for beams B2, B3, and B4, respectively, which is almost constant. However, the first shear cracking loads showed significant variations. It can be noticed that increasing the perforation size resulted in decrease the first shear cracking load as presented

in Table 5. For all Perforation beams, the mode of failure was shear failure at the first web-post as depicted in Figs 4 (b-g).

It is worth mentioning that, for all perforated beams, the solid parts adjacent to both end supports were almost constant in order to eliminate shear failure near supports. In addition, the width of web-post was constant for all perforated beams. Therefore, since the loading pattern was the same, the position of acting load varied according to the perforation size. Thus, the concrete section at the shear span zone showed significant variations for the three perforated beam. Accordingly, the shear stress was resisted by two web-posts for beam B2 as depicted in Fig. 4(c), while it resisted by one web-post for beams B3 and B4. Despite that the distance from the acting load to the center of the web-post for beams B3 and B4 is different. Accordingly, the beam B2 resisted higher loading compared to that resisted by beams B3 and B4. Thus the shear failure of beam B2 was more stringent than that exhibited by beams B3 and B4 as shown in Fig. 4(c, e and g).

In sum, the shear capacity of the perforated beam is strongly influenced by the perforation size as well as the distance of the acting to center of the first web-post.

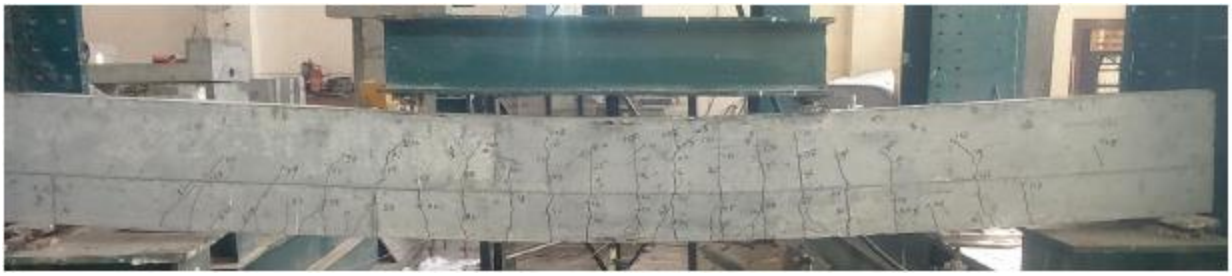

(a) Beam B1

(b) Beam B2

)c) Zone A of Beam B2

(d) Beam B3

(e) Zone B of Beam B3

(f) Beam B4

(g) Zone C of Beam B4

Fig.4: Failure modes of all beams.

Load-deflection response

Figure 5 shows comparisons among the applied jacking load versus the corresponding mid-span deflection along the entire loading history for all beams. It can be noticed that the solid control beam B1 sustained three cycles before complete failure. On the other hand, the perforated beams sustained either two cycles as for beams B2 and B3 or one cycle as for beam B4. As shown in Fig. 5, all beams showed identical response at low loading level, however, with further loading the stiffness of the perforated beams started to degrade leading to increased mid-span deflection. The developed deflection of the control beam B1 at complete failure was extremely high compared to the exhibited ones of the perforated beam. That could be attributed to the sudden shear failure of all perforated beams. Although, two beams (B2 and B3) sustained ultimate load higher than that manifested by the control solid beam B1. The percentages of increases are 10.7% and 1.2% for beams B2 and B3, respectively. That could be attributed to the contribution of the added longitudinal bars above and below the perforations. However, beam B4 that provided by 200 mm by 400 mm rectangular perforations failed to reach the same ultimate capacity of the solid beam.

Based on the section analysis of both solid section and the perforated section provided by side reinforcement above and below the perforations as depicted in Fig. 1(e), it was found that the flexural resistance of the perforated section is higher than that of the corresponding solid section by about 33%. Thus, if the perforated beam was perforated only at the middle zone subjected to pure bending moment only the ultimate capacity would be increased by about 33%. On the other hand, if perforations were provided in the shear zone, the shear strength would be decreased taking into account the size of the perforations as well as the relative distance between the acting load and the center of the web-post. Accordingly, the overall ultimate capacity of the perforated beam is influence by the flexural ultimate capacity gain and the decrease in the shear resistance. Based on the experimental resistances of the control solid beam along with the perforated beam, it could be

concluded that the decreases in the shear capacity due to the provided perforations are 22.3%, 31.8% and 49.8%, respectively, for beams B2, B3, and B4.

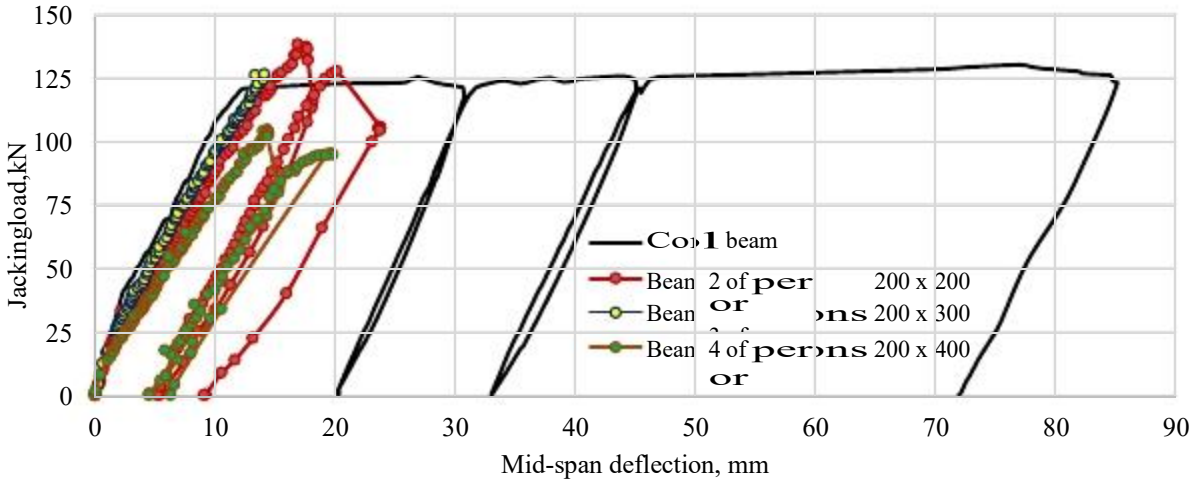

Fig.5: Comparison among load-deflection relationships for all beams.

Based on manifested modes of failures for all perforated beams, the perforated beams can be modeled as analogous vierendeel girders. The total span and the shear spans are the same for all beams, however, the solid parts near the support zones as well as the distance between the web-posts are different. The solid parts near supports are modeled as small bays in order to keep the same typical span for the first perforation. Each vierendeel girder is analyzed linearly under the effect of the ultimate sustained loads obtained from the experimental tests. Thus, the total load acted on beams B2, B3 and B4 are 138.4, 126.5 and 104.0 kN, respectively. Fig. 6 shows the developed shear force diagrams along all members for the analogous vierendeel girders. It could be observed that the maximum stressed members due to shear are the same web-posts failed experimentally, which gives some confidence on the results of the analogous vierendeel girders. In addition, inspite that the variations of the acting loads are 9% (B2, B3) and 25% (B2, B4), the variations of the developed shear forces are 8.5% and 0.5%, respectively. Thus, the ultimate shear stresses for the three beams considering the effective depth of 120 mm and width of the section is 150 mm are 3.5, 3.8 and 3.4MPa, respectively, for beams B2, B3 and B4. These values are higher than the concrete shear strength (about 1.7 MPa).

The failure pattern of all beams are in complete agreement with the results of the analogous vierendeel where horizontal cracks were developed at the junction of the web-post and the upper chord. In addition, since the web-posts did not have horizontal reinforcement, these web-posts failed due to shear stress where the web-posts provided their shear resistance by the concrete and the dowel action of the longitudinal bars. More refined shear model is undergoing and its outcomes will be found elsewhere.

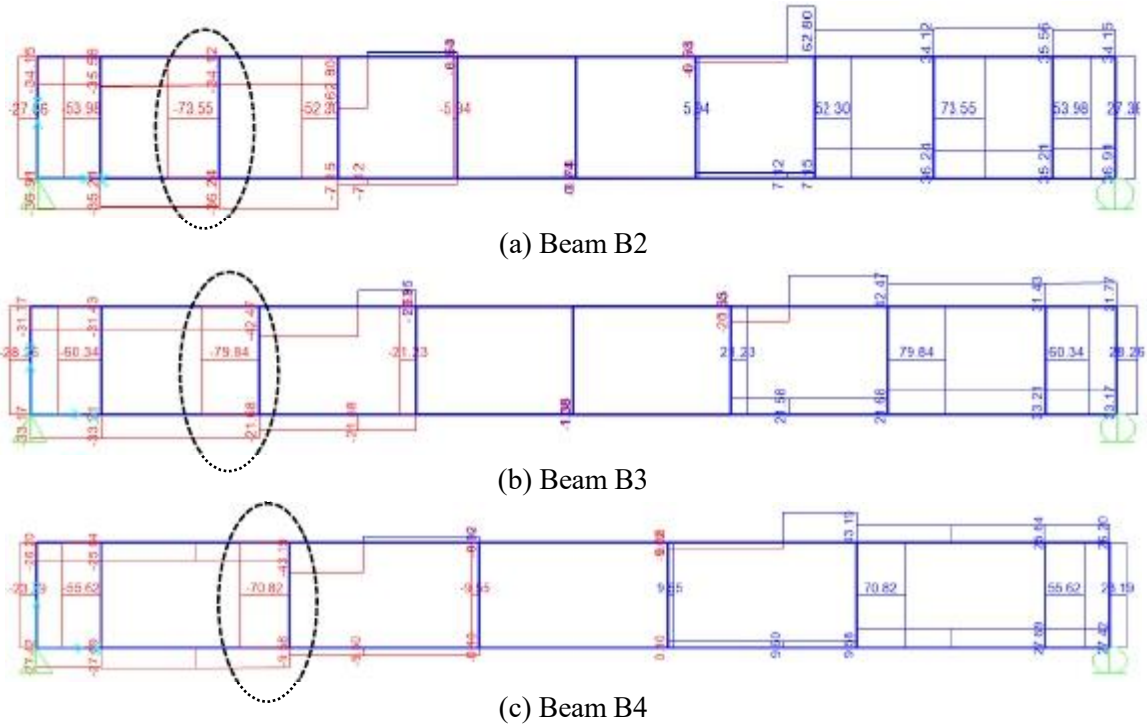

(a) Beam B2

(b) Beam B3

(c) Beam B4

Fig.6: Developed shear force diagrams for all perforated beams based on analogous vierendeel girders.

Ultimate tensile strains

The developed normal strain on the longitudinal steel bars were recorded at different locations as shown in Fig. 1. However, the developed tensile normal strain near the mid-span region is compared for all beams. Based on the material properties of the used steel bars, the yielding strain is 2072 micro-strain. As shown in Fig. 6, the developed strain on the main steel of the control solid beam exceeded the yielding point and entered the plastic zone. Therefore, after unloading of the first cycle, the main steel bars retained higher strain value greater than the yielding strain. Thus, for the following cycles the strain values were greater than the yielding point. On the other hand, for all perforated beams, the first cycles were ended while the developed tensile strain on the main steel were lower than the yielding point. Accordingly, the retailed permanent tensile strains after unloading were lower than the yielding strain owing to the retailed permanent plastic deflection after unloading.

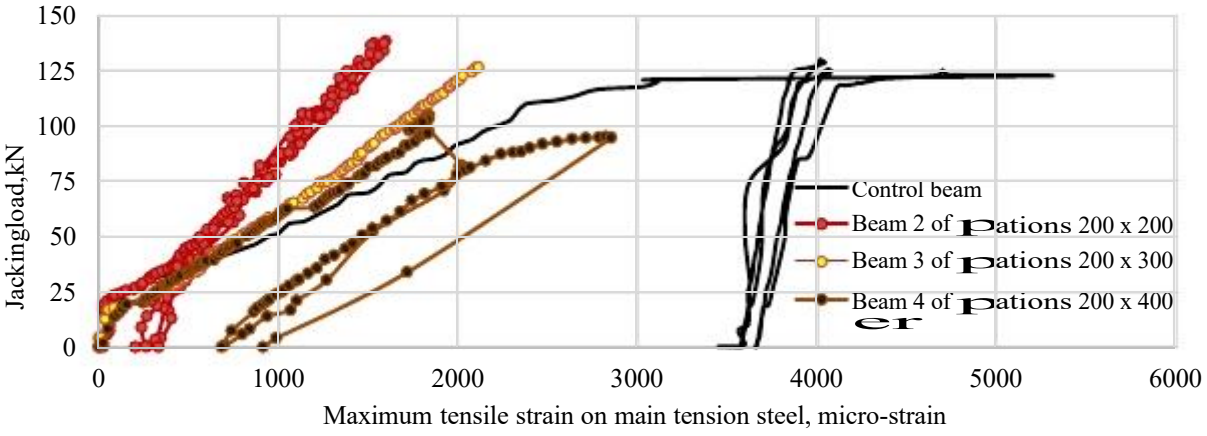

Fig.6: Comparison among load-tensile strain relationships for all beams.

Comparison among the performance of all beams

In order verify the efficiency of the developed perforation system, all perforated beams are compared against the control solid beam considering the manifested ultimate capacity and the relative cost. Table 6 summaries the controlling parameters for all perforated beams as well as the control solid beam. It is worth mentioning that the total cost of all beams was calculated based on the local prices of the used materials at the time of casting the beams considering only the cost of the used material assuming constant labor cost for all beams.

It could be noticed that the saving in the overall cost is inversely proportional to the gain in the ultimate capacity of the perforated beam. That means the increases in the dimensions of the perforations resulted in more mass loss and more cost saving on the expense of the manifested ultimate capacity. For practical use, providing rectangular perforations of dimensions 200 x 300 mm resulted in cost saving of about 8% and slight increase in the ultimate capacity of about 1.2%. On contrary, providing square perforations of side length of 200 mm resulted in ultimate capacity gain of about 10.7% while the total cost reduced by about 3%. That is based on the adopted reinforcement configurations. On the other hand, providing rectangular perforations of dimensions 200 x 400 resulted in 11% saving in the overall cost, however, the provided reinforcement configurations could not enabled the perforated beam to sustain ultimate capacity as that of the solid beam. Thus, proper reinforcement configuration/ strengthening technique is required.

Table 6: Controlling parameters for all perforated beams.

Beam	Concrete volume reduction	Concrete volume, m^3	Reinforcement weight, kg			Ultimate capacity gain	Relative cost compared to control beam
			Long* steel	Stirrups	Total		
B1	0.0	0.210	17.58	12.6	30.2	NA	1.00
B2	24.2%	0.157	26.10	10.4	36.5	10.7%	0.97
B3	28.6%	0.150	26.10	8.69	34.8	1.2%	0.92
B4	30.7%	0.146	26.10	7.82	33.9	-16.8%	0.89

*Long steel includes main tension and compression reinforcements along with additional longitudinal steel above and below the perforations; **the cost of material are calculated based on the actual prices of steel reinforcement and concrete ingredients at the time of conducting the experimental program; negative sign means decrease.

CONCLUSION

Experimental program was conducted in order to evaluate the structural behavior of reinforced self-compacted reinforced concrete beams with rectangular perforation. Within the scope of this study the following conclusions may be drawn:

- Sharp edge perforations trigger shear failure at the first web-post for all perforation sizes provided that no shear reinforcement is provided.
- Perforated beams using rectangular perforations could outperform their ultimate capacities compared to that of the solid control beam. However, an efficient detailing or strengthening configuration is required in order to eliminate the developed shear failure.

REFERENCES

- Ahmed, A., Fayyadh, M. M., Naganathan, S., Nasharuddin, K., (2012), "Reinforced concrete beams with web opening", ELSEVIER, Vol. 40, pp. 90-102.
- Mansur, M. A., Tan, K.H., (1999), "Concrete Beams With Openings Analysis and Design ", Boca Raton London New York Washington, D.C.
- Siddhalingesh, B. K., Eramma, H., (2016) "Experimental Investigation on Internally Strengthened RC Beam with Rectangular Web Opening" International Journal of Innovative Research in Science, Engineering and Technology Vol. 5, No. 8, pp. 15410-15417 .
- Mansur, M. A., Hasnat, A., (1979), "Concrete Beams with Small Opening under Torsion", Proceedings, American Society of Civil Engineers, Vol. 105(ST 11), pp. 2433-2447.
- Somes, N. F., Corley, W.G., (1974), "Circular openings in webs of continuous beams". American Concrete Institute. Detroit, MI, pp. 359-398.
- Mustafa B. Dawood, Haider H. A. Al-Katib , (2015). "Flexural Strength of Prestressed Concrete Beams with Openings and Strengthened with CFRP Sheets" INTERNATIONAL JOURNAL OF SCIENTIFIC & TECHNOLOGY RESEARCH Vol. 4, No. 6, pp.161-172.
- Okamura, H., (1999), "Self-Compacting High Performance Concrete", Social System Institute, Tokyo (in Japanese)
- Chai, H.W., (1998), "Design and testing of self-compacting concrete", PhD thesis, Department of Civil and Environmental Engineering, University College London.
- El-Reedy, M. A. (2009), "Advanced Materials and Techniques for Reinforced Concrete Structures". CRC Press.
- Shetty, M. S. (2005), "Concrete technology: Theory and practice". Ram Nagar, New Delhi: S. Chand & Company.
- Specification and Guidelines for self-compacting concrete – EFNRC, Association House, 99 West Street, Fordham, survey GU 97 EN, U.K.